Two-Site Adsorption Model for the ($\sqrt{3} \times \sqrt{3}$)-R30° Dodecanethiolate Lattice on Au(111) Surfaces

Xavier Torrelles,[†] Carolina Vericat,[‡] María Elena Vela,[‡] Mariano H. Fonticelli,[‡] María Antonieta Daza Millone,[‡] Roberto Felici,[§] Tien-Li Lee,[||] Jorg Zegenhagen,[||] Guadalupe Muñoz,[⊥] José A. Martín-Gago,[⊥] and Roberto C. Salvarezza*[,‡]

Instituto de Ciencia de los Materiales de Barcelona−CSIC, Campus de Bellaterra, Spain, Instituto de Investigaciones Fisicoquímicas Teóricas y Aplicadas (INIFTA), CONICET-UNLP, Casilla de Correo 16 Suc. 4, 1900 La Plata, Argentina, INFM-OGG, c/o ESRF, BP 220 Grenoble, France, European Synchrotron Radiation Facility, BP 220, F-38043 Grenoble, France, and Instituto de Ciencia de Materiales de Madrid−CSIC, Campus de Cantoblanco, 28049 Madrid, Spain

Received: August 29, 2005; In Final Form: January 24, 2006

The surface structure of dodecanethiolate self-assembled monolayers (SAMs) on Au(111) surfaces, formed from the liquid phase, have been studied by grazing incidence X-ray diffraction (GIXRD), scanning tunneling microscopy (STM), and electrochemical techniques. STM images show that the surface structure consists of ($\sqrt{3} \times \sqrt{3}$)-R30° domains with only a few domains of the c(4 × 2) lattice. The best fitting of GIXRD data for the ($\sqrt{3} \times \sqrt{3}$)-R30° lattice is obtained with alkanethiolate adsorption at the top sites, although good fittings are also obtained for the fcc and hcp hollow sites. On the basis of this observation, STM data, electrochemical measurements, and previously reported data, we propose a two-site model that implies the formation of incoherent domains of alkanethiolate molecules at top and fcc hollow sites. This model largely improves the fitting of the GIXRD data with respect to those observed for single adsorption sites and, also, for the other possible two-site combinations. The presence of alkanethiolate molecules adsorbed at the less favorable top sites could result from the adsorption pathway that involves an initial physisorption step which, for steric reasons, takes place at on top sites. Once the molecules are chemisorbed, the presence of energy barriers for alkanethiolate surface diffusion, arising mostly from chain−chain interactions, "freezes" some of them at the on top sites, hindering their movement toward fcc hollow sites. By considering the length of the hydrocarbon chain and the adsorption time, the two-site model could be a tool to explain most of the controversial results on this matter reported in the literature.

1. Introduction

Self-assembled monolayers (SAMs) can be described as single layers of highly oriented, ordered, and packed molecules adsorbed on a substrate. Among them, SAMs of alkanethiols ($X(CH_2)_nSH$) on metals are of great scientific interest because they provide an easy method to create well-defined surfaces with controllable chemical functionalities. The possible applications of SAMs range from nanotechnology to fundamental surface science. In particular, SAMs of alkanethiols on gold can be used to modify wetting and wear properties of solid surfaces, to develop nanodevices for electronics, and for pattern formation.[1] Also, by anchoring specific chemical groups to these molecular self-assemblies, well-ordered structures with a wide variety of chemical functionalities can be employed in molecular recognition, protein adsorption, and as templates for crystallization of inorganic salts, among others.[1,2]

The self-assembly process can occur both in gas-phase and in liquid environments (from solutions of different solvents), the latter being the most popular method because of its simplicity and accessibility in most laboratories. This process implies chemisorption of the molecules on the Au surface through the S heads, forming strong alkanethiolate bonds.[3] The interaction between the neighbor hydrocarbon chains also plays an important role in the self-assembly process.[4] The resulting stable surface structures for samples prepared both from the gas-phase environment and by solution deposition consist mainly of ordered domains of the ($\sqrt{3} \times \sqrt{3}$)-R30° and the so-called c(4 × 2) superlattice of the ($\sqrt{3} \times \sqrt{3}$)-R30° lattice (better described as ($3 \times 2\sqrt{3}$)rect) [5], which coexist with vacancy Au islands of mono- or di-atomic height, commonly known as "pits".[6]

One of the most controversial points in the study of alkanethiolates on Au(111) is the nature of the adsorption site (or sites) involved in the different stable alkanethiolate surface structures mentioned above. The knowledge of the actual adsorption site(s) is not only an academic problem but is also an important issue with practical implications. This knowledge is relevant for molecular electronics and, also, for electron transfer to redox species and biomolecules immobilized on SAMs that can be used in sensors and biosensors. In fact, it has been shown that the conductance of a single-thiol molecule changes with the adsorption site.[7] The presence of different adsorption sites could also explain the wide scatter observed in molecular conductance measurements for alkanethiolate molecules on Au(111).[8]

* Corresponding author.
[†] Instituto de Ciencia de los Materiales de Barcelona−CSIC.
[‡] Instituto de Investigaciones Fisicoquímicas Teóricas y Aplicadas (INIFTA).
[§] INFM-OGG.
[||] European Synchrotron Radiation Facility.
[⊥] Instituto de Ciencia de Materiales de Madrid−CSIC.

10.1021/jp054879m CCC: $33.50
Published on Web 03/01/2006

The ($\sqrt{3} \times \sqrt{3}$)-R30° and c(4×2) lattices have been studied by a wide range of techniques. While the ($\sqrt{3} \times \sqrt{3}$)-R30° lattice exhibits nearest neighbor distances between the S heads of 5 Å, its c(4×2) superlattice presents some displacement of the S heads from the positions found for the ($\sqrt{3} \times \sqrt{3}$)-R30° lattice, as revealed by grazing incidence X- ray diffraction (GIXRD),[9,10] X- ray standing waves (XSW),[11] and scanning tunneling microscopy (STM) data,[12] hence yielding a surface structure with two different adsorption sites. However, even for the simpler ($\sqrt{3} \times \sqrt{3}$)-R30°, where all surface sites are equivalent, the specific adsorption site of the thiolate molecule is under debate, as discussed below.

Density functional theory (DFT) calculations have been widely used to predict the most favorable adsorption sites of alkanethiolates on Au(111).[13] However, the DFT calculations performed by different research groups for methanethiolate (CH_3S) on Au(111) yield completely different results, probably due to the presence of local energy minima.[13] Therefore, hcp, bridge, fcc, fcc-bridge, and hcp-bridge sites have all been regarded as the preferred sites for alkanethiolate adsorption on the Au(111) face.

Very recently, however, two unexpected experimental results have been reported: X-ray photoelectron diffraction (XPD)[14] and normal incidence XSW[15] studies of ($\sqrt{3} \times \sqrt{3}$)-R30° methanethiolate lattices on Au(111) formed from the gas phase independently found that thiolate adsorption would take place at on-top sites. It should be noted that all DFT calculations agree on the fact that the adsorption energy of alkanethiolate molecules at top sites is the smallest (less favorable) among the usually considered Au(111) sites.[13]

Also, the quality of alkanethiolate SAMs is essential for many of their technological applications and this is closely related to the adsorption kinetics, which strongly depends on the assembly procedure (gas phase or liquid phase), adsorption time, thiol concentration or exposure, and hydrocarbon chain length, among others.[16,17] Many such studies have been performed, and a wide range of results, some of them contradictory, have been attained. Among them, for gas-phase formed SAMs, physisorbed species have been found at low temperatures with UHV techniques,[18] as well as ordered domains of flat-lying alkanethiolate molecules by in situ STM (not clearly detected for SAMs prepared in liquid environments), previous to the formation of the ordered islands of vertically oriented molecules.[19] Adsorption kinetics data for assembly from solution are more difficult to interpret due to the presence of the solvent, among other factors.[16,17]

From the above discussion, it is clear that the determination of the adsorption sites for alkanethiolates on the Au(111) surface remains an open issue that deserves further investigation. In particular, it would be important to determine the adsorption sites for long-chain ($n > 10$) alkanethiolate SAMs on Au(111), since those are the ones that exhibit a small number of defects (they form crystallinelike adlayers), and to study the SAMs formed from ethanolic solutions, because this is the self-assembly route mostly used in chemical laboratories. Also, it should remain clear that kinetic aspects cannot be disregarded as they play a fundamental role in the formation of SAMs and surface structure.

In this paper, we present GIXRD data for the ($\sqrt{3} \times \sqrt{3}$)-R30° dodecanethiolate ($CH_3(CH_2)_{11}S$, DT) SAMs on Au(111) prepared from solution deposition. The best fitting of the GIXRD data results for alkanethiolate adsorption at top sites, although good fittings are also observed for models with alkanethiolate adsorption on fcc or hcp hollow sites. On the basis of this result, STM images, electrochemical measurements, previously reported experimental data, and theoretical calculations from the literature, we propose a two-site model for dodecanethiolate adsorption. This model, involving domains of alkanethiolate species at fcc and top sites that are incoherent and equally populated, largely improves the GIXRD data fitting with respect to the single site models. The two-site model reconciles DFT calculations and experimental data by introducing kinetic considerations. The presence of DT molecules at these two sites can be explained by the existence of physisorbed species at on-top sites, which then become chemisorbed and can eventually diffuse to the more favorable fcc sites. This last step depends on the energy barrier arising from the van der Waals interactions between adjacent molecules and could be the reason for finding domains of "frozen" DT species at on-top sites in addition to domains of molecules at the more stable fcc hollow configuration. Therefore, this model suggests that the study of the surface structure of alkanethiolates on Au(111) should involve not only typical surface physics structure measurements but also the consideration of the complex physical chemistry involved in the overall adsorption process. This integrated view could explain the discrepancies mentioned in the literature and open a question about the final equilibrium state of these most interesting, and intriguing, two-dimensional systems.

2. Experimental Section

Au(111) single crystals (MaTeck, Germany), prepared in an ultrahigh vacuum (UHV) by several heating and sputtering cycles, were used as substrates for GIXRD measurements. Au thin films on glass (AF 45 Berliner Glass KG, Germany) prepared by evaporation were used as substrates for STM imaging and for most electrochemical measurements. After annealing for three minutes with a hydrogen flame, these Au substrates exhibit atomically smooth (111) terraces separated by mono-atomic steps in height.[20] The self-assembled monolayer was prepared following the usual protocol described in the literature.[4] After surface preparation, the Au substrates were immersed in 5×10^{-5} M dodecanethiol ($CH_3(CH_2)_{11}SH$) ethanolic solutions for 24 h to yield a complete SAM and, then, were rinsed with ethanol to remove weakly adsorbed molecules. The DT-covered substrates were then used for X-ray diffraction measurements or for STM imaging. For electrochemical measurements, substrates were modified in 5×10^{-7} M dodecanethiol ethanolic solutions with adsorption times of 2−100 min.

STM imaging was made in air in the constant current mode with a Nanoscope III microscope from Digital Instruments (Santa Barbara, CA) and by using commercial Pt−Ir tips. Typical tunneling currents, bias voltages, and scan rates were 0.2 nA, 900 mV, and 6 Hz, respectively. Steps present in the Au(111) surface (2.4 Å in height) were used to calibrate the piezo-tube in the *z*-direction.

Cyclic voltammetry (total interfacial capacitance and reductive electrodesorption) measurements were made in a conventional 3-electrode glass cell at 25 °C using the DT-covered electrodes as the working electrode, a Pt large area wire as the counter electrode, and a saturated calomel electrode (SCE) as the reference electrode. All potentials are referred to the SCE. The scan rate was 0.05 V s^{-1}. In all cases, the electrolyte solution was aqueous 0.1 M NaOH degassed just before the measurements. The surface coverage of the chemisorbed DT was calculated by measuring the charge density of the electroreduction peak.[21] The total DT surface coverage was estimated from total interfacial capacitance measurements in the double layer potential region of the voltammogram.[22,23]

The GIXRD measurements were carried out at ID32 beamline at the ESRF and were performed in a vacuum chamber mounted on a six-circle diffractometer in a vertical geometry (i.e., with the normal of the sample in the vertical direction). The X-ray energy was set to 11.0 keV with the incoming beam fixed to the critical angle of the substrate (0.36°) during the whole experiment. A total of 309 reflections were measured, which were reduced to 195 nonequivalent ones after their average by considering $p3$ symmetry and a mirror plane along the [1,0] gold-substrate direction. The residual between equivalent reflections was of about 15%. The (2,0,0.9) reflection of the $(\sqrt{3} \times \sqrt{3})$-R30° superstructure was measured at regular time intervals to monitor the sample degradation due to radiation damage. The intensity of this reflection decreased following an exponential decay with a lifetime of about 5.5 h; for this reason, data were always acquired on newly prepared samples. The X-ray exposure time for each sample was lower than 5 h. During this period of time, the control reflection diminished its intensity by a factor 2, approximately. The entire data set was renormalized to this reference reflection, which was measured during the entire experiment.

The gold crystal was not described with the standard cubic basis of lattice parameter $a_o = 4.08$ Å but, instead, with a hexagonal basis (a_1, a_2, a_3) with a_1 and a_2 in the (111) surface plane (a_1 and a_2 are equal to the nearest-neighbor surface distance $a_o/\sqrt{2}$) and a_3 perpendicular to the surface ($a_3 = \sqrt{3}a_o$). The corresponding reciprocal lattice vectors are directed along the three axes H, K, and L with H and K in the surface plane forming an angle of 60° and L normal to the surface. With this basis, bulk Bragg reflections are found at $(H, K) = (1, 0)$, $L = 1, 4, 7, \ldots$ and $(H, K) = (0, 1)$, $L = 2, 5, 8$. For simplicity, we have re-indexed them to the $(\sqrt{3} \times \sqrt{3})$-R30°, using the transformation matrix:

$$(H, K)_{\sqrt{3}\times\sqrt{3}} = (H, K)_{(1\times1)}\begin{pmatrix} 2 & -1 \\ 1 & 1 \end{pmatrix}$$

$(H, K)_{(1\times1)}$ being the film reflections indexed with respect to the substrate basis.

The lattice parameters of the $(\sqrt{3} \times \sqrt{3})$-R30° surface cell are the following: $a = b = 4.99$ Å, $c = \sqrt{3}a_o$, $\alpha = \beta = 90°$, and $\gamma = 120°$. The unit cell contains one molecule. Note that, obviously, all the reflections of the $(\sqrt{3} \times \sqrt{3})$-R30° coincide with reflections of the c(4 × 2) superstructure; i.e., they are common to both structures.

The intensity modulation of the (2, 1) and (0, 2) reflections common to both the c(4 × 2) and $(\sqrt{3} \times \sqrt{3})$-R30° superstructures along the perpendicular momentum transfer direction showed their equivalence within the experimental error bar. This equivalence is explained by considering three $(\sqrt{3} \times \sqrt{3})$-R30° domains rotated 120° between them plus a mirror plane along the [1, 0] direction as consequence of the $p3m1$ symmetry of the gold substrate, which increases the number of total domains of the $(\sqrt{3} \times \sqrt{3})$-R30° superstructure to six. The plane group symmetry experimentally observed is consequently $p31m$.

3. Results and Discussion

3.1. DT Surface Structure on Au(111). A typical STM image (73 × 73 Å^2) of the DT-covered Au(111) substrate is shown in Figure 1a. The molecules form a hexagonal array (inset in Figure 1a) with nearest-neighbor distances $d \approx 5$ Å, consistent with the $(\sqrt{3} \times \sqrt{3})$-R30° lattice. A 300 × 300 Å^2 STM image (Figure 1b) taken at a lower resolution on a large Au(111) terrace completely covered by the $(\sqrt{3} \times \sqrt{3})$-R30° lattice shows domains with different contrast (blue and green) and large

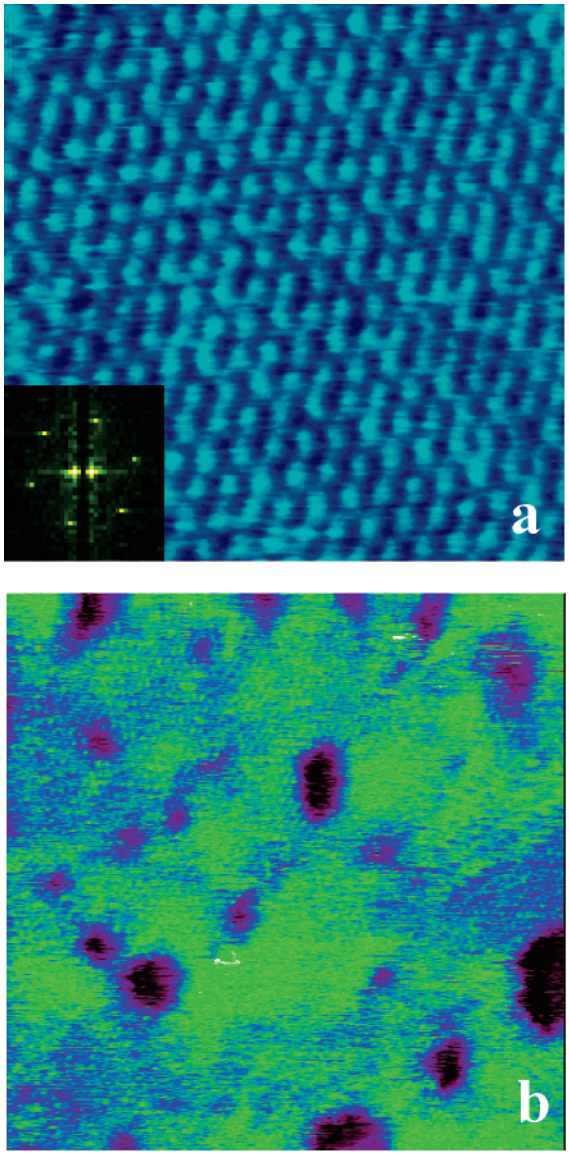

Figure 1. (a) 73 × 73 Å^2 STM image of the dodecanethiolate-covered Au(111) substrate showing the $(\sqrt{3} \times \sqrt{3})$-R30° lattice. (inset) Fourier transform of the image. (b) 300 × 300 Å^2 image at lower resolution of a large Au(111) terrace completely covered by the $(\sqrt{3} \times \sqrt{3})$-R30° lattice. Domains with different contrast can be clearly observed.

holes (magenta−black regions). The large holes correspond to the typical gold mono-atomic or di-atomic high vacancy islands (pits), with the bottom of the pits also covered by alkanethiolate molecules.[24] Also, the molecular domains (green−blue) spread on the terrace without a defined shape and with typical domain sizes ranging from 80 to 150 Å. The difference in contrast between adjacent molecular domains corresponds to a height difference ≈ 0.3−0.6 Å, too low to be assigned to the Au substrate topography. A detailed analysis of the STM images taken at different places of the substrate only shows traces of the c(4 × 2) superlattice. We have imaged a few small domains of this superlattice embedded into the $(\sqrt{3} \times \sqrt{3})$-R30° lattice. In fact, in the particular case of DT SAMs, the amount of the c(4 × 2) superlattice is smaller than that of the $(\sqrt{3} \times \sqrt{3})$-R30° lattice. This fact agrees with previous observations for decanethiolate[9] and hexadecanethiolate[10] self-assembled on Au(111) where annealing of the samples was needed to obtain a reasonable amount of c(4 × 2) (about 40%). Conversely, we have found that the c(4 × 2) structures dominate for hexanethiolate on Au(111),[25] while it is known that open lattices (striped

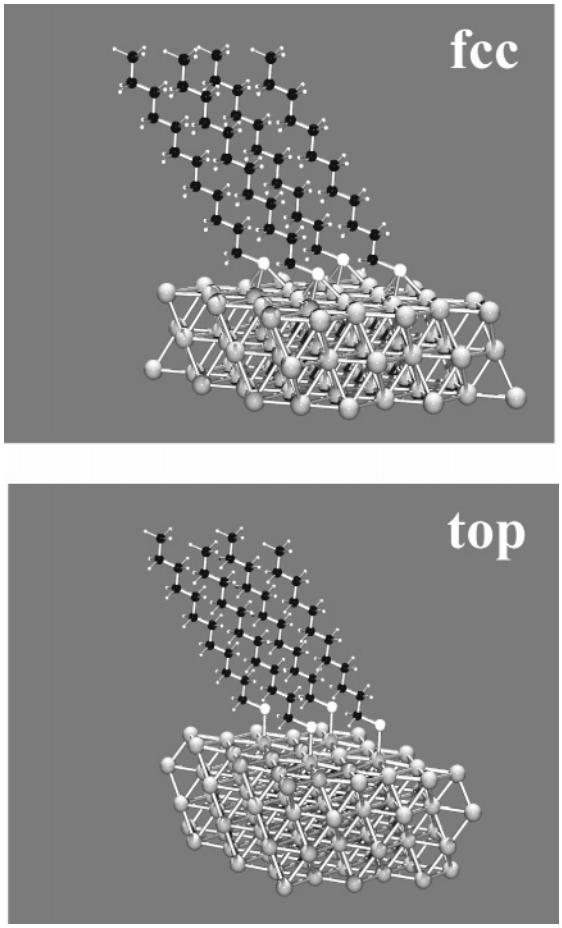

Figure 2. Side view of the best fit to the structure for fcc-hollow and top sites. The gold substrate has been laterally expanded to better visualize the Au−S connectivity. Gray, white, and black colors correspond to gold, sulfur, and carbon atoms, respectively. Small white circles stand for hydrogen atoms.

phases) and some unstable surface structures are commonly found for shorter thiolates[26,27] on Au(111).

3.2. GIXRD Data: Single Site Adsorption Model. In regards to the GIXRD measurements, we have measured the full width at half-maximum (fwhm) of the rocking curves of two reflections of the ($\sqrt{3} \times \sqrt{3}$)-R30° structure versus time. The fwhm of reflections (1, 0) and (2, 0) practically remain constant with time during the whole experiment, since their widths vary from 2.0 to 2.1° and 1.0 to 1.1°, respectively, which means that surface degradation takes place in a statistical way inside the domain. From these peak widths, the minimum terrace size corresponds approximately to 120 Å, a figure that is consistent with STM images.

To elucidate the correct structure we have fitted the experimental GIXRD data by using a modified version of the ROD program,[28] which permits the user to consider each DT chain as a rigid block. The independent chains, centered on the sulfur atom, were allowed to rotate (three degrees of freedom defined by the Eulerian angles ϕ, θ, and ψ) around their (y, z) internal axis in Cartesian coordinates. They were transformed to crystallographic coordinates after each rotation (Eulerian angles). These angles (see Figure 2 of ref 10 for a sketch and angle definition) can also be defined as a twist angle about the hydrocarbon chain axis (ϕ), a tilt angle with respect to the surface normal (θ), and a precession or azimuthal angle in the surface plane (ψ). Moreover, the thiol molecule was allowed to move within the $\sqrt{3} \times \sqrt{3}$ surface cell by using three new (x, y, z) parameters to explore bridge connectivity between sulfur and neighbor gold atoms. The atoms of the six topmost surface gold layers were also allowed to relax laterally as well as along the z-axis of the surface cell.

TABLE 1: Goodness of the Fit (χ^2) of the Models Considering Different Adsorption Sites

model	top	fcc	hcp	bridge	incoherent (fcc−top)
χ^2	1.8	2.0	2.2	2.4	1.3

Substrate relaxations must be considered due to the high atomic number of the gold atoms. In fact, since small variations from their ideal positions produced non-negligible contributions to the calculated intensities and resulted in playing an important role in the fit procedure, the six topmost surface layers were permitted to relax. The number of gold structural parameters was 18, while DT molecules involved a total of 4 parameters plus one scale factor. Two temperature parameters were also used to simulate the same linear dependence of the vibration amplitude along the chain for all molecules (see below).

A linear vibration amplitude along the chain was introduced to reduce the amplitude of the oscillations appearing in the calculated fractional order rods when ideal DT chains were considered. The period (T) of these oscillations is a function of the projected chain length ($T = L \sin \theta$, with L being the chain length). Since these oscillations were not experimentally observed in the fractional order rods, rather big vibration amplitudes are expected to affect the chains, which, on the other hand, allow us to obtain the indetermination of the averaged molecular tilt angle. The Debye Waller (DW) dependence along the chain was supposed to be linear with the z-coordinate of each atom: $B(z) = B_{\text{init}} + (B_{\text{end}} - B_{\text{init}})z/L$ where B_{init} is the Debye Waller value for the S atom and B_{end} is the corresponding value for the further C atom in the chain (defined as $B = 8\pi^2\langle u^2\rangle$, where $\langle u^2\rangle$ is the thermal average of the squared atomic displacements).

The agreement factors from the structure refinement for the top and fcc models,[28] where the previous DW dependence was considered, were very similar; i.e., $\chi^2 = 1.8$ and 2.0, respectively (Table 1). The model considering the S atom in the hcp position gives a χ^2 value of 2.2, while the bridge one gives a value around 2.4. The model considering the fcc-bridge position, suggested as the most favorable adsorption site in recent DFT calculations,[13i] has also been analyzed. When the alkanethiolate molecule is forced to be in the fcc-bridge position and the gold atoms are relaxed, the fit of the experimental data leads to a χ^2 value of 2.1. This value slightly drops to 2.0 if the position of the molecule is also permitted to relax. However, in this case, the molecule shifts toward the fcc position. The change in χ^2 between both positions is very small, but the refinement process shows that the fcc-bridge position is not stable during this procedure.

3.3. Why is a Two-Site Adsorption for Dodecanethiolate on Au(111) Possible? After inspection of Table 1, we conclude that, in terms of χ^2, on-top is the most probable site for dodecanethiolate adsorption, although the goodness of the fitting for fcc or even hcp sites is also acceptable. This is an interesting result that clearly contrasts with previous experimental data, where only top sites were considered.[14] Therefore, the results from Table 1 open a new question: is alkanethiolate adsorption on two sites in the Au(111) surface possible? We have considered this possibility based on different observations: (1) The STM images in Figure 1b show domains with small differences in STM contrast. Although this has been assigned to differences in the orientation of the alkyl chains of the

TABLE 2: Relative Coordinates of the Surface Atoms for the Two Proposed Adsorption Sites

element	*x*/*a* (±0.004) top	*y*/*b* (±0.004) top	*z*/*c* (±0.005) top	*x*/*a* (±0.004) 3-fold	*y*/*b* (±0.004) 3-fold	*z*/*c* (±0.005) 3-fold
S	0	0	1.327	0	0	0.590
Au-11	0	0	1 (−0.019)			
Au-12	2/3	1/3	1 (−0.045)			
Au-13	1/3	2/3	1 (−0.043)			
Au-21	1/3 (−0.004)	1/3 (−0.001)	2/3 (−0.016)			
Au-31	2/3 (+0.006)	2/3 (+0.001)	1/3 (−0.008)	2/3 (−0.011)	2/3 (−0.014)	1/3 (+0.035)
Au-41	0	0	0 (−0.002)	0	0	0 (+0.027)
Au-42	2/3	1/3	0 (−0.007)	2/3	1/3	0 (+0.017)
Au-43	1/3	2/3	0 (−0.003)	1/3	2/3	0 (+0.017)

alkanethiolates,[29] adsorption on different sites cannot be discarded. In fact, one can speculate that these domains correspond to the incoherent domains composed by alkanethiolate molecules placed at on-top and hollow sites and that the 0.3−0.6 Å difference in height between the domains in Figure 1b could correspond to the height difference between DT molecules placed at top and hollow sites, although one should bear in mind that STM images contain both electronic and topographic contributions.[30] To evaluate whether these figures are unrealistic, we have measured the height difference between the bright and dark spots of the c(4 × 2) superlattice (where the presence of two nonequivalent sites is widely accepted) for different alkanethiols and from a large number of STM images. We have found values in the range of 0.2−0.4 Å that, in principle, could be assigned to the height (contrast) difference between the fcc and hcp sites.[10] Thus, the 0.3−0.6 Å height difference seems to be reasonable for alkanethiols adsorbed at top and hollow sites. (2) As mentioned before, soft annealing of long-chain alkanethiolate SAMs (as those shown in Figure 1) results in a transformation from the ($\sqrt{3} \times \sqrt{3}$)-R30° lattice to the c(4 × 2) surface structure. Recent GIXRD data taken on the latter are consistent with molecules placed at fcc hollow sites.[10] Reversible ($\sqrt{3} \times \sqrt{3}$)-R30° ↔ c(4 × 2) transformations have also been observed by real-time STM imaging of alkanethiolate domains on Au(111).[12,25] Therefore, if one accepts top sites for the ($\sqrt{3} \times \sqrt{3}$)-R30° lattice and fcc hollow sites for the c(4 × 2) lattice, the transformation from ($\sqrt{3} \times \sqrt{3}$)-R30° → c(4 × 2) could involve ($\sqrt{3} \times \sqrt{3}$)-R30° domains at top and hollow sites. (3) High-resolution electron energy loss spectroscopy (HREELS)[31a] and also sum frequency generation (SFG) data[31b] for different alkanethiolates adsorbed on Au(111) show multiple or single site adsorption depending on the hydrocarbon chain length. (4) Rectangular (4 × $\sqrt{3}$) lattices with a molecular tilt of 50° have been recently observed for long-chained alkanethiols on the Au(111) face at nonsaturated coverage by AFM.[32a] The same structure has also been imaged by STM for propanethiolate and annealed hexanethiolate SAMs on Au(111).[32b] This lattice that clearly involves two different substrate sites evolves toward the ($\sqrt{3} \times \sqrt{3}$)-R30° lattice at higher surface coverages.

3.4. Analysis of the GIXRD Data for the Two-Site Model. We have now different evidence (points 1−4) suggesting that the coexistence of domains of ($\sqrt{3} \times \sqrt{3}$)-R30° in two different sites is a possible alternative for dodecanethiolate adsorption on Au(111). Therefore, we have re-analyzed our GIXRD data in terms of a two-site adsorption model. First, we explored the possible models that result from Table 1 by considering a coherence coexistence of two adsorption sites, i.e., molecules in different adsorption sites that coexist randomly in the same domain. The models obtained from the coherent combination of two adsorption sites use more fitting parameters than those models based on a single adsorption site since the different adsorption sites of the two thiol molecules can induce different local relaxations, so the gold atoms of the two topmost layers are permitted to relax independently. The two subsystems formed by a molecule and the two topmost gold layers are equally populated. The models resulting from the coherent combination of molecules in different adsorption sites from Table 1 always give χ^2 values larger than those obtained from models using only a single adsorption site. For this reason, these types of coherent models were disregarded. However, by considering an incoherent coexistence of top and fcc S sites on the surface (the sites that individually yield the minimum χ^2 values) with equal population, as derived from the best adjustment, χ^2 significantly drops to 1.3. Other combinations were also explored, but in all cases, the χ^2 values were significantly higher. The incoherent coexistence model also has a larger number of parameters than the 3-fold or top models individually, since the two topmost gold layers of each model have been allowed to relax independently (as in the coherent case). The χ^2 of the fit for the checked models summarized in Table 1 were obtained with the in-plane S-coordinates fixed to their ideal positions, and only the *z*-coordinate was allowed to vary. When the in-plane coordinates of the S atoms are allowed to move with respect to their ideal positions, the displacements are lower than 0.5 Å, while their χ^2 values remain close to those shown in the previous table. The angular rotations of the DT molecules for each configuration, however, were kept identical: $\phi = 172°$ (±3°), $\theta = 34°$ (±2°), and $\psi = 6°$ (±2°).

Table 2 shows the atomic coordinates and displacements of both incoherent surface terminations. The in-plane atomic displacements for the top model are very small and can be considered to be included in their respective error bars. The total number of parameters used in our best fit was consequently: 18 (*x*, *y*, *z*) parameters (top model), 6 (*x*, *y*, *z*) parameters (3-fold model), 3 rotation angles for the dodecanethiol molecule plus 2 vertical displacements for each of them, 2 temperature factors, and 1 scale factor. The two topmost surface layers of the 3-fold model were refined independent of those of the top model, but deeper layers, i.e., layers 5 and 6 of both models, were relaxed identically. The relaxations of layers 5 and 6 were very small and corresponded to average vertical displacements of 0.05 and 0.03 Å, respectively. Deeper layers were disregarded because their displacements were already included in their respective error bars. A representation of these two different adsorption sites is presented in Figure 2. From Table 1, we observe different behaviors for both surface terminations. The in-plane relaxations of the top model are negligible, while the surface normal direction exhibits a compression that diminishes its value with depth. However, the 3-fold model shows larger in-plane relaxations for the topmost surface layer, while atoms expand along the vertical direction.

The tilt of DT chains is around 34°, and the closest C−Au distance is 2.9 Å for the 3-fold model. The S−Au distances are very similar (identical attending to their respective error bars, ±0.1 Å) for both surface terminations: 2.35 and 2.44 Å for the 3-fold and top models, respectively. The distances from S to the planes defined by the topmost surface gold layers are 1.56 and 2.57 Å for the 3-fold and top models, respectively.

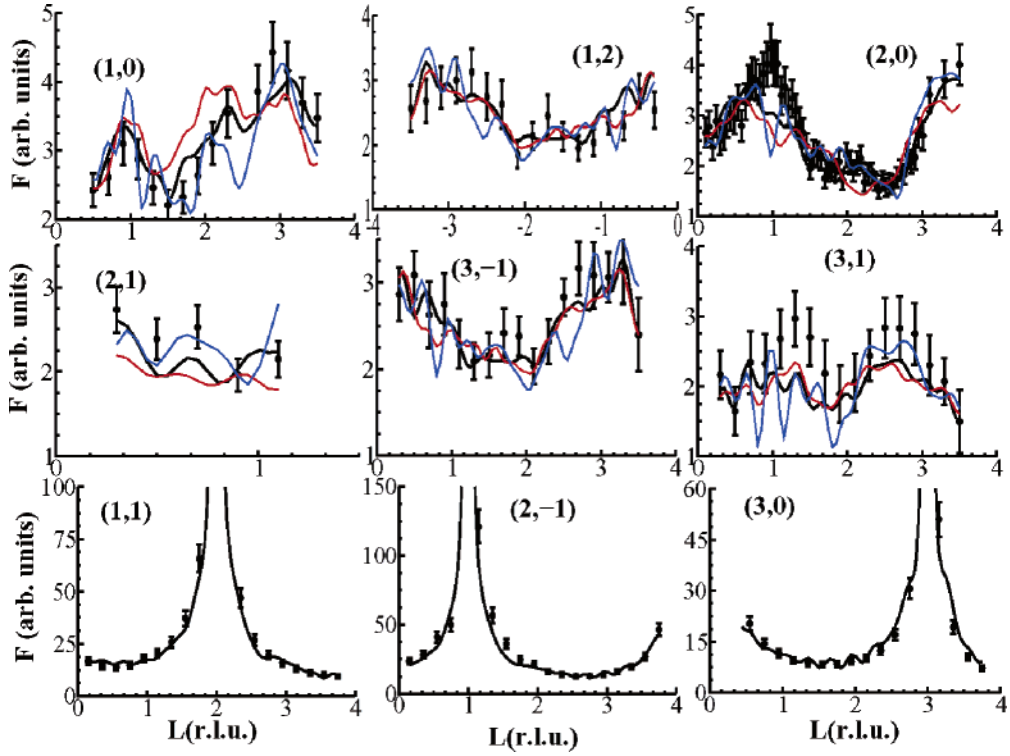

Figure 3. Experimental structure factors vs perpendicular momentum transfer L for six different fractional order rods structure (top and middle) plus three CTRs (bottom). Theoretical calculations for different models (continuous lines) according to the structure depicted in Figure 2 (including gold relaxations) are shown: individual fcc (red), individual top (blue), and incoherent two-domain fcc−top (black).

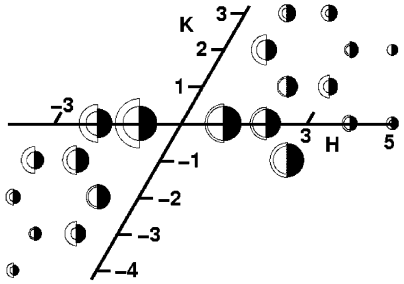

Figure 4. In-plane reflections. The radii of the empty semicircles are proportional to the measured in-plane structure factors of the ($\sqrt{3} \times \sqrt{3}$)-R30° reconstruction; the uncertainties in the data are indicated by the two radii. The filled semicircles are proportional to the calculated structure factors with the model displayed in Figure 2.

The comparison between experimental and theoretical data obtained from the fit refinement procedure considering the two surface incoherent termination models is shown in Figures 3 and 4. The in-plane data is shown with $p3$ symmetry to visualize the experimental equivalence between equivalent reflections. Figure 3 shows the theoretical calculations obtained from the individual fcc (continuous red line) and top (continuous blue line) models, while the continuous black line shows the calculated values from the incoherent two-domain (fcc−top) model. The crystal truncation rods (CTRs) only show the calculated data obtained from the incoherent model. The (2, 0, L) fractional order rod was measured in the stationary mode type as well as in the rocking mode type.[33] For this reason, the number of points of this rod is larger. Other incoherent models considering combinations of the individual fcc, top, hcp, or bridge models grouped by pairs were also checked. The χ^2 value that was obtained from them was always higher than 1.7. Although the differences in terms of χ^2 between our best model (top−fcc) and the other incoherent combinations are not very strong, other structural artifacts have to be taken into account during the discrimination procedure of the best model. The S−Au distance does not remain stable during the fit procedure in these new models, giving distances that are either too short (in the case of models including the bridge possibility) or too large (for the other cases). Consequently, the best χ^2 value in these new models was always obtained by fixing the S−Au distance to a value of 2.4 Å.

In regards to the Debye Waller factors of the thiol chains, B_{init} takes a value of 4, while B_{end} takes a value of 70, which correspond to average vibration amplitudes of 0.2 and 0.9 Å, respectively.[10] That means that S atoms are well localized in the unit cell while C atoms could be more delocalized due to radiation damage that likely reduces the average chain length of the molecules in a statistical manner.

Despite the fact that the two-site model has a larger number of parameters than the 3-fold or top models individually, as explained before, the two-site model is physically feasible and cannot be discarded. In particular, this model offers an alternative to solve the apparent controversy between DFT calculations and experimental data.

3.5. Possible Explanation for the Two-Site Adsorption Model. The presence of two adsorption sites might be surprising, but the interplay between thermodynamics and kinetics must be always kept in mind. The presence of separate ($\sqrt{3} \times \sqrt{3}$)-R30° domains with molecules at on-top sites and at fcc hollow sites could be explained by considering the possible adsorption pathway of the alkanethiol molecules. There is some experimental evidence of a physisorbed state presence in the gas phase on Au(111)[18] and Cu(111).[34] Some theoretical calculations suggest that physisorption takes place at on-top sites of metal surfaces due to steric reasons.[13b,i] Although some works have suggested the existence of a physisorbed phase in solution from atomic force microscopy (AFM) measurements[35,36] and from the re-adsorption curve of cyclic voltammograms,[37] it is evident that only a technique able to discriminate the nature of the S

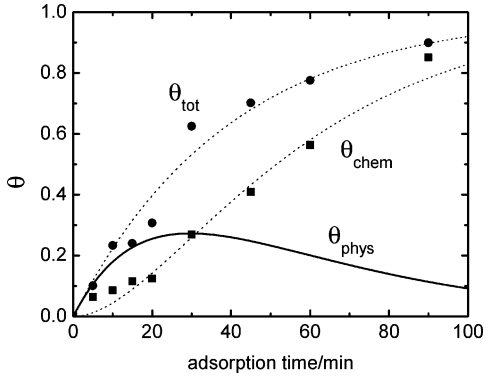

Figure 5. Coverage vs time curves obtained from the electrochemical measurements: (circles) experimental total coverage from capacitance measurements; (squares) experimental chemisorbed species coverage from reductive electrodesorption curves; (solid line) coverage of physisorbed species. The dotted lines are guides for the eye.

metal bond is required. The use of cyclic voltammetry and, in particular, the combination of total interfacial capacitance and reductive electrodesorption measurements are good tools for this purpose because this allows us to measure the total amount of adsorbate and the amount of the adsorbate that has transferred charge to the substrate by electrodesorption curves (i.e., the chemisorbed species), respectively.

We have estimated the surface coverage of chemisorbed alkanethiolates and that of total adsorbed species by cyclic voltammetry measurements performed on the same sample. The measurements were done for many samples and for different adsorption times. The procedure was the following: A gold sample is dipped in a very diluted thiol solution (5×10^{-7} M) for adsorption times t between 2 and 100 min and, then, is carefully rinsed. The samples are then placed as working electrodes in the electrochemical cell with 0.1 M NaOH solution, and the cyclic voltammograms are performed.

The total thiol coverage θ_{tot} (physisorbed + chemisorbed) is calculated from the total interfacial capacitance C. It is well-known that the capacitances of alkanethiolate self-assembled monolayers are approximately 1 order of magnitude smaller those of bare gold electrodes. C is almost constant with potential and can be obtained by dividing the charging current density j by the scan rate υ in a potential range where no faradaic processes (oxidation or reduction reactions) occur.[22] C was calculated for different adsorption times, and the capacitances C_{mono} of a full thiolate monolayer (24 h incubation) and that of a bare gold electrode (C_0) were also calculated, all in the same electrolyte. Then, the total coverage $\theta_{tot} = (C(t) - C_0)/(C_{mono} - C_0)$.

On the other hand, the thiolate desorption reaction is $Au-SC_{12}H_{25} + 1e^- \rightarrow Au + C_{12}H_{25}S^-$. The charge involved in the desorption process, $q_{chem}(t)$, can be calculated by integration of the desorption peak.[21] A complete monolayer (24 h incubation) yields a charge density $q_{chem,mono} \approx 90\ \mu C\ cm^{-2}$. The fraction of chemisorbed molecules can be calculated as $\theta_{chem} = q_{chem}(t)/q_{chem,mono}$.

Then, for each adsorption time, the difference between θ_{tot} and θ_{chem} is θ_{phys}. This coverage corresponds to thiol molecules that are not chemisorbed (they are not thiolates and, thus, cannot be reduced to thiol molecules), but still, they are adsorbed on the gold electrode because they affect the value of the capacitance.

In Figure 5, we have plotted θ_{tot} and θ_{chem} calculated from our voltammetric measurements. It is clear that at the initial stages of the adsorption process θ_{tot} largely exceeds θ_{chem} indicating the presence of physisorbed species. Therefore, in Figure 5, we have included θ_{phys} estimated from the difference $\theta_{phys} = \theta_{tot} - \theta_{chem}$. Note that both phases can coexist at relatively high coverage on the Au surface ($\theta_{phys} = \theta_{chem} = 0.4$). This is important experimental evidence supporting the coexistence of both physisorbed and chemisorbed species for a relatively long period of time during the adsorption pathway of dodecanethiolate on Au(111).

There is both experimental and theoretical evidence indicating that R−SH and SH_2 species are adsorbed on metal surfaces at top sites due to the steric hindrance introduced by the H atoms.[13b,i,38] In the case of alkanethiols on Au(111), it has been reported that they adsorb at on-top sites with the C−S plane parallel to the substrate. Therefore, physisorption and the initial stage of chemisorption (with loss of the H atoms) should take place at on-top sites. If the van der Waals interactions among the neighbor hydrocarbon chains (1 Kcal mol^{-1} C-$unit^{-1}$)[39] are not stronger than the energy barrier from the on-top to the energetically more favorable fcc hollow sites (6 Kcal mol^{-1}),[13f] then an on-top thiolate could diffuse to an adjacent fcc hollow site and a domain with S heads in fcc sites could nucleate. For long alkanethiolates, one should expect that this process takes place when the on-top chemisorbed molecule does not have neighbors. Conversely, diffusion of the on-top chemisorbed molecules to the more favorable fcc sites should be hindered when two or more chemisorbed molecules at adjacent top sites are present. In this case, a domain of molecules with the S heads at top sites is formed. Therefore, the fcc/top ratio should be determined at the initial stage of the adsorption process because in densely covered surfaces the chain−chain interactions prevent diffusion to other sites. The fcc/top ratio ≈ 1, derived from the best fit for the experimental data, should be interpreted considering that, statistically, the same probability for the initial adsorption of isolated or adjacent molecules exists. The importance of chain−chain interactions can be experimentally appreciated in a decrease of 2 orders of magnitude in the surface mobility of Au atoms in the presence of alkanethiolates (10^{-17} $cm^2\ s^{-1}$ vs 10^{-15} $cm^2\ s^{-1}$ for Au without adsorbed thiolates), as has been already reported.[12b] The decrease in the Au surface mobility induced by hydrocarbon chain−hydrocarbon chain interactions could explain why the amount of the c(4×2) lattice, which involves fcc and hcp sites,[10] is reduced as the hydrocarbon chain length increases; i.e., the molecules can reach more stable adsorption sites because they are more mobile. For long-chained alkanethiolates, the on-top domains can be frozen in this "metastable" state for a long period of time. The only way to induce surface mobility is by sample annealing, but in this case, the ($\sqrt{3} \times \sqrt{3}$)-R30° lattice transforms directly to the c(4×2) lattice.[10]

Moreover, short adsorption times (and, in general, experiment time windows too short to attain the equilibrium structures) would result in thiolates adsorbing preferentially at on-top sites. This could perhaps explain recent results for methanethiolate SAMs[14,15] and reveals the importance of the time as a variable to be taken into account in adsorption processes. However, it must be pointed out that, in refs 14 and 15, adsorption was done in high vacuum (the dosing is done maybe for a couple of hours), while our samples were incubated for 24 h. Moreover, even if the adsorption times were the same, adsorption in solution and in the gaseous phase could be different (due to the presence of the solvent, for example) and thus equilibrium could be reached at different times.

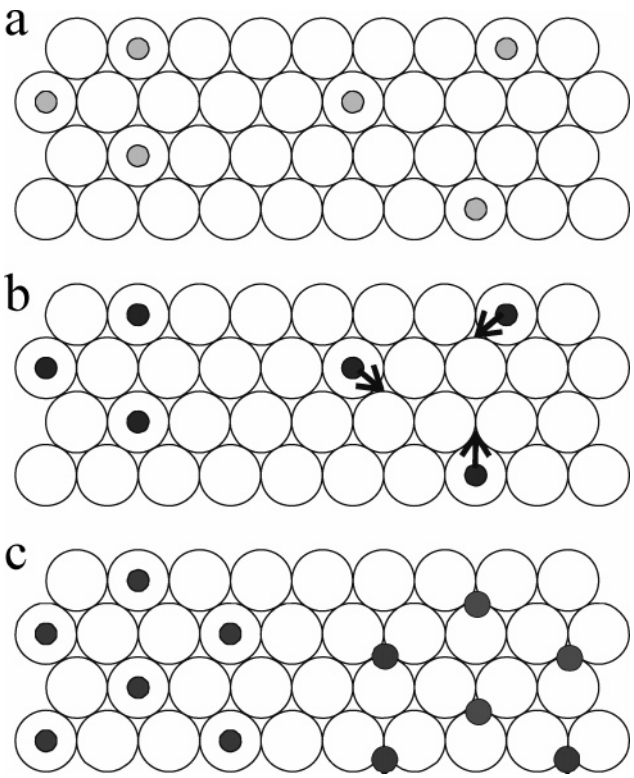

Figure 6. Scheme showing the formation of two different types of surface domains of alkanethiolate species on Au(111). (a) Alkanethiol physisorption at on-top sites. (b) Alkanethiolate chemisorption (with loss of mercaptan hydrogen) at on-top sites. The arrows indicate surface diffusion of noninteracting molecules to the more stable fcc sites. (c) Two domains corresponding to on-top and fcc hollow sites

The proposed reaction pathway for alkanethiol adsorption on the metal surface can be represented by a scheme showing the different steps in the adsorption process (Figure 6): (a) First, alkanethiol molecules physisorb at on-top sites; (b) then, on-top alkanethiol molecules lose the mercaptan hydrogen and on-top alkanethiolate chemisorption occurs. If a chemisorbed molecule at an on-top site does not have near neighbors, it can move to an adjacent fcc site (see arrows in part b). Around this molecule, an fcc domain can be created (right domain in part c). On the other hand, if a chemisorbed molecule at a top site has a neighbor molecule, chain−chain interaction freezes these molecules there so that an on-top domain is formed (left domain in part c). Thus, depending on the substrate temperature, surface coverage and hydrocarbon chain length, and also on time, different populations of molecules adsorbed at different adsorption sites could be reached on the Au(111) surface.

Finally, it should be noted that, from recent DFT calculations,[13i,40] alkanethiolate adsorption should take place at fcc-bridge sites of the Au(111) surface. In contrast, the best fit for our experimental data results for top and fcc (single site adsorption model) and fcc−top (two-site adsorption model). However, adsorption at fcc-bridge sites from DFT calculations has been found for relatively short alkanethiolates where the substrate influence on the whole molecule should be strong. Moreover, these short-chained alkanethiolates have been preferentially selected to perform DFT calculations on these systems due to the well-known failure of DFT to describe dispersion forces present in long-chained alkanethiolates,[41] i.e., chain−chain interactions, which influence the adsorption site. Therefore, the extrapolation of results obtained from DFT calculations for short alkanethiolates has to be considered with care for longer molecules due to these oversimplifications.

4. Conclusion

The surface structure of the ($\sqrt{3} \times \sqrt{3}$)-R30° dodecanethiolate on Au(111) prepared by solution deposition by the usual protocol has been investigated by GIXRD. The X-ray data give similar χ^2 goodness of the fit for top and hollow sites. However, this value drops when considering the possibility of two coexisting alkanethiolate adsorption sites, top and fcc, on the gold surface. This two-site model is compatible with STM images and also with previously reported data from different techniques. The presence of chemisorbed alkanethiolates at the less favorable top sites could result from an adsorption pathway involving an initial physisorption, as detected by electrochemical measurements, and from the presence of energy barriers for alkanethiol surface diffusion. This energy barrier that increases as the surface coverage and the length of the hydrocarbon chain increases could freeze some alkanethiolates species at on-top sites. As the surface mobility of the molecules is slow, time also plays an important role in the final surface structure obtained. Therefore, according to the hydrocarbon chain length, coverage, time window of the experiment, and temperature, the alkanethiolates in the ($\sqrt{3} \times \sqrt{3}$)-R30° lattice on Au(111) can be placed at on-top or at fcc sites or both.

The physical picture emerging from this model for long-chain alkanethiolates SAMs prepared from solution deposition consists of a ($\sqrt{3} \times \sqrt{3}$)-R30° surface structure forming small domains, with molecules at different sites, some of them trapped in some kind of metastable state. This picture could be important when this type of sample is used as a building block for the preparation of molecular systems and devices. The existence of the metastable state (together with the fact that most theoretical calculations are done for very short thiolates) could explain why density functional theory fails to predict the actual adsorption sites for the ($\sqrt{3} \times \sqrt{3}$)-R30°, as DFT applies only to equilibrium structures. Therefore, the two-site model could explain most of the recent controversial results on this matter.

Acknowledgment. We are grateful to the Spanish M.C.yT. Agency for partially funding this project through projects MAT2002-00395 and MAT2002-02808 and to the Argentinian ANPCyT (PICT-02-11111 and PICT-03-17492). M.E.V. is a member of the research career of CIC (Bs. As.). C.V. acknowledges a grant from Fundación Antorchas.

References and Notes

(1) Wilbur, J. L.; Whitesides, G. M. *Nanotechnology*; Timp, G., Ed.; Springer Verlag: New York, 1999; Chapter 8. Haag, R.; Rampi, A. M.; Holmlin, R. E.; Whitesides, G. M. *J. Am. Chem. Soc.* **1999**, *121*, 7895−7906. Lio, A.; Charych, D. H.; Salmeron, M. *J. Phys. Chem. B* **1997**, *101*, 3800−3805.

(2) Castner, G.; Ratner, B. D. *Frontiers in Surface and Interface Science*; Duke, C. B., Plummer, E. W., Eds.; North-Holland: Amsterdam, 2002; p 28. Cunningham, A. *Introduction to Bioanalytical Sensors*; Wiley-Interscience: New York, 1998.

(3) Nuzzo, R. G.; Zegarski, B. R.; Dubois, L. H. *J. Am. Chem. Soc.* **1987**, *109*, 733−740. Vericat, C.; Vela, M. E.; Andreasen, G.; Salvarezza, R. C.; Vazquez, L.; Martin-Gago, J. A. *Langmuir* **2001**, *17*, 4919−4924.

(4) Ulman, A. *Chem. Rev.* **1996**, *96*, 1533−1554.

(5) Widrig, C. A.; Alves, C. A.; Porter, M. D. *J. Am. Chem. Soc.* **1991**, *113*, 2805−2810. Dubois, L. H.; Zegarski, B. R.; Nuzzo, R. G. *J. Chem. Phys.* **1993**, *98*, 678−688. Fenter, P.; Eisenberger, P.; Liang, K. S. *Phys. Rev. Lett.* **1993**, *70*, 2447−2450. Camillone, N., III; Chidsey, C. E. D.; Liu, G.-Y.; Scoles, G. *J. Chem. Phys.* **1993**, *98*, 3503−3511.

(6) Bucher, J.-P.; Santesson, L.; Kern, K. *Langmuir* **1994**, *10*, 979−983. Poirier, G. E.; Pylant, E. D. *Science* **1996**, *272*, 1145−1148.

(7) Basch, H.; Ratner, M. A. *J. Chem. Phys.* **2003**, *119*, 11926−11942.

(8) Labonte, A. P.; Tripp, S. L.; Reifenberger, R.; Wei, A. *J. Phys. Chem. B* **2002**, *106*, 8721−8725. Reifenberger, R. SPM-based Measurements of Molecular Conduction. Presented at NSF-CONICET Quilmes Nanoscience Workshop, Tucumán, Argentina, May 2003.

(9) Fenter, P.; Eberhardt, A.; Eisenberger, P. *Science* **1994**, *266*, 1216−1218.

(10) Torrelles, X.; Barrena, E.; Munuera, C.; Rius, J.; Ferrer, S.; Ocal, C. *Langmuir* **2004**, *20*, 9396−9402.

(11) Fenter, P.; Schreiber, F.; Berman, L.; Scoles, G.; Eisenberger, P.; Bedzyk, M. J. *Surf. Sci.* **1998**, *412/413*, 213−235.

(12) Terán Arce, F.; Vela, M. E.; Salvarezza, R. C.; Arvia, A. J. *J. Chem. Phys.* **1998**, *109*, 5703−5706. (b) Terán Arce, F.; Vela, M. E.; Salvarezza, R. C.; Arvia, A. J. *Electrochim. Acta* **1998**, *44*, 1053−1067.

(13) Beardmore, K. M.; Kress, J. D.; Bishop, A. R.; Grønbech-Jensen, N. *Synth. Met.* **1997**, *84*, 317−318. Beardmore, K. M.; Kress, J. D.; Grønbech-Jensen, N.; Bishop, A. R. *Chem. Phys. Lett.* **1998**, *286*, 40−45. (b) Grönbeck, H.; Curioni, A.; Andreoni, W. *J. Am. Chem. Soc.* **2000**, *122*, 3839−3842. (c) Yourdshahyan, Y.; Zhang, H. K.; Rappe, A. M. *Phys. Rev. B* **2001**, *63*, 081405R. (d) Vargas, M. C.; Gianozzi, P.; Selloni, A.; Scoles, G. *J. Phys. Chem. B* **2001**, *105*, 9509−9513. (e) Hayashi, T.; Morikawa, Y.; Nozoye, H. *J. Chem. Phys.* **2001**, *114*, 7615−7621. (f) Akinaga, Y.; Nakajima, T.; Hirao, K. *J. Chem. Phys.* **2001**, *114*, 8555−8564. (g) Gottschalck, J.; Hammer, B. *J. Chem. Phys.* **2002**, *116*, 784−790. (h) Yourdshahyan, Y.; Rappe, A. *J. Chem. Phys.* **2002**, *117*, 825−833. (i) Cometto, F. P.; Paredes-Olivera, P.; Macagno, V. A.; Patrito, E. M. *J. Phys. Chem. B* **2005**, *109*.

(14) Kondoh, H.; Iwasaki, M.; Shimada, T.; Amemiya, K.; Yokohama, T.; Ohta, T.; Shimomura, M.; Kono, S. *Phys. Rev. Lett.* **2003**, *90*, 066102.

(15) Roper, M. G.; Skegg, M. P.; Fisher, C. J.; Lee, J. J.; Dhanak, V. R.; Woodruff, D. P.; Jones, R. G. *Chem. Phys. Lett.* **2004**, *389*, 87−91.

(16) Schreiber, F. *Prog. Surf. Sci.* **2000**, *65*, 151−257. Schreiber, F. *J. Phys.: Condens. Matter* **2004**, *16*, R881−R900.

(17) Schwartz, D. K. *Annu. Rev. Phys. Chem.* **2001**, *52*, 107−137.

(18) Lavrich, D. J.; Wetterer, S. M.; Bernasek, S. L.; Scoles, G. *J. Phys. Chem. B* **1998**, *102*, 3456−3465. Schreiber, F.; Eberhardt, A.; Leung, T. Y. B.; Schwartz, P.; Wetterer, S. M.; Lavrich, D. J.; Berman, L.; Fenter, P.; Eisenberger, P.; Scoles, G. *Phys. Rev. B* **1998**, *57*, 12476−12481.

(19) Yamada, R.; Uosaki, K. *Langmuir* **1998**, *14*, 855−861. Poirier, G. E.; Fitts, W. P.; White, J. M. *Langmuir* **2001**, *17*, 1176−1183.

(20) Andreasen, G.; Vela, M. E.; Salvarezza, R. C.; Arvia, A. J. *Langmuir* **1997**, *13*, 6814−6819.

(21) Widrig, C. A.; Chung, C.; Porter, M. D. *J. Electroanal. Chem.* **1991**, *310*, 335−359.

(22) Finklea, H. O. *Electroanalytical Chemistry*; Bard, A. J., Rubinstein, I., Eds.; Marcel Dekker: New York, 1996; Vol 19, pp 109−335.

(23) Damaskin, B. B.; Petri, O. A.; Batrakov, V. V. *Adsorption of Organic Compounds on Electrodes*; Plenum Press: New York, 1971; p 114.

(24) McDermott, C. A.; McDermott, M. T.; Green, J. B.; Porter, M. D. *J. Phys. Chem.* **1995**, *99*, 13257.

(25) Vericat, C.; Andreasen, G.; Vela, M. E.; Martin, H.; Salvarezza, R. C. *J. Chem. Phys.* **2001**, *115*, 6672−6678.

(26) Benítez, G.; Vericat, C.; Tanco, S.; Remes Lenicov, F.; Castez, M. F.; Vela, M. E.; Salvarezza, R. C. *Langmuir* **2004**, *20*, 5030−5037.

(27) Hagenstrom, H.; Schneeweiss, M. A.; Kolb, D. M. *Langmuir* **1999**, *15*, 2435−2443. Petri, M.; Kolb, D. M.; Memmert, U.; Meyer, H. *Electrochim. Acta* **2003**, *49*, 175−182.

(28) Vlieg, E. *J. Appl. Crystallogr.* **2000**, *33*, 401−405.

(29) Zeng, C.; Li, B.; Wang, B.; Wang, H.; Wang, K.; Yang, J.; Hou, J. G.; Zhu, Q. *J. Chem. Phys.* **2002**, *117*, 851.

(30) *Scanning Tunneling Microscopy and Related Methods*; Behm, R. J., Garcia, N., Rohrer, H., Eds.; NATO ASI Series; Kluwer Academic Publishers: Dordrecht, 1990.

(31) (a) Kato, H.; Noh, J.; Hara, M.; Kawai, M. *J. Phys. Chem. B* **2002**, *106*, 9655−9658. (b) Yeganeh, M. S.; Dougal, S. M.; Polizzotti, R. S.; Rabinowitz, P. *Phys. Rev. Lett.* **1995**, *74*, 1811−1814.

(32) (a) Barrena, E.; Palacios-Lidón, E.; Munuera, C.; Torrelles, X.; Ferrer, S.; Jonas, U.; Salmeron, M.; Ocal, C. *J. Am. Chem. Soc.* **2004**, *126*, 385. (b) Vericat, C.; Vela, M. E.; Salvarezza, R. C. *Phys. Chem. Chem. Phys.* **2005**, *7*, 3258−3268.

(33) Torrelles, X.; Rius, J. *J. Appl. Crystallogr.* **2004**, *37*, 395−398.

(34) Jackson, G. J.; Woodruff, D. P.; Jones, R. G.; Singh, N. K.; Chan, A. S. Y.; Cowie, B. C. C.; Formoso, V. *Phys. Rev. Lett.* **2000**, *84*, 119−122.

(35) Xu, S.; Cruchon-Dupeyrat, S. J. N.; Garno, J. C.; Liu, G.-Y.; Jennings, G. K.; Yong, T.-H.; Laibinis, P. E. *J. Chem. Phys.* **1998**, *108*, 5002−5012.

(36) Barrena, E.; Ocal, C.; Salmeron, M. *J. Chem. Phys.* **2001**, *114*, 4210.

(37) Yang, D.-F.; Wilde, C. P.; Morin, M. *Langmuir* **1996**, *12*, 6570−6577. (b) Byloos, M.; Al-Maznai, H.; Morin, M. *J. Phys. Chem. B* **1999**, *103*, 6554−6561.

(38) Sellers, H. *Surf. Sci.* **1993**, *294*, 99−107.

(39) Israelachvili, J. N. *Intermolecular and Surface Forces*; Academic Press: London, 1994; pp 353 and 408.

(40) Morikawa, Y.; Hayashi, T.; Liew, C. C.; Nozoye, H. *Surf. Sci.* **2002**, *507−510*, 46−50.

(41) Krystián, S.; Pulay, P. *Chem. Phys. Lett.* **1994**, *229*, 175−180.